Received: 18 May 2020 | Revised: 22 September 2020 | Accepted: 30 September 2020

DOI: 10.1002/cta.2893

ORIGINAL PAPER

WILEY

A study of amplitude-to-phase noise conversion in planar oscillators

Torsten Djurhuus | **Viktor Krozer**

Institute of Physics, Goethe-University Frankfurt, Frankfurt am Main, Germany

Correspondence
Torsten Djurhuus, Institute of Physics, Goethe-University Frankfurt, Max-von-Laue-Str. 1 , 60438 Frankfurt am Main, Germany.
Email: t.djurhuus@physik.uni-frankfurt.de

Funding information
Deutsche Forschungsgemeinschaft, Grant/Award Number: KR 1016/16-1

Summary

This paper explores the many interesting implications for oscillator design, with optimized phase-noise performance, deriving from a newly proposed model based on the concept of oscillator conjugacy. For the case of 2-D (planar) oscillators, the model prominently predicts that only circuits producing a perfectly symmetric steady-state can have zero amplitude-to-phase (AM-PM) noise conversion, a so-called zero-state. Simulations on standard industry oscillator circuits verify all model predictions and, however, also show that these circuit classes cannot attain zero-states except in special limit-cases which are not practically relevant. Guided by the newly acquired design rules, we describe the synthesis of a novel 2-D reduced-order LC oscillator circuit which achieves several zero-states while operating at realistic output power levels. The potential future application of this developed theoretical framework for implementation of numerical algorithms aimed at optimizing oscillator phase-noise performance is briefly discussed.

KEYWORDS

AM-PM noise conversion, circuit analysis, nonlinear dynamical systems, oscillators, phase noise, system analysis and design

1 | INTRODUCTION

Oscillator jitter is an unavoidable consequence of the internal noise sources generated by circuit components operating at room temperature. The effects of oscillator jitter are observed in the frequency domain as a broadening of the phase-noise spectrum. This issue represents a serious design obstacle as it for example causes inter-channel interference in communication systems which in turn results in increased bit error rates (BERs). The reduction of close-to-carrier phase-noise hence remains one of the most critical and essential factors of any oscillator design project.

A portion of the oscillator phase-noise response originates from amplitude perturbations which are then modulated into the phase in a process known as *oscillator AM-PM noise conversion*.[1-9] Herein, the following expression, $D = D_{\phi\phi} + D_{\phi a}$, for the *phase-diffusion*, D, is introduced. The phase-diffusion is a real parameter which entirely characterizes the phase-noise response of an autonomous oscillator.[10-12] The contributions $D_{\phi\phi}$ and $D_{\phi a}$ are the oscillator phase-diffusion constants due to phase (PM) and amplitude (AM) noise, respectively. Hence, $D_{\phi a}$ quantifies the AM-PM noise conversion of the oscillator in a single constant. Importantly, this AM-PM component, $D_{\phi a}$, is not a static quantity but rather a function of the oscillator topology and chosen parameter values. An example illustrating this fact

can be found in Djurhuus et al[8,9] which considered a quadrature oscillator (QVCO) circuit. That paper revealed AM-PM noise conversion to be a consequence of nonlinear coupling between oscillator blocks hence suggesting that the AM-PM noise conversion could theoretically be canceled by introducing linear coupling.

The QVCO example highlights the appealing idea that the AM-PM contribution can be viewed as an "additional" contribution which could, potentially, by some clever engineering or concepts (in the above case linear coupling), be canceled or at least minimized. Hence, through optimized circuit design, it should then be possible to at least reduce, if not cancel, the phase-diffusion component $D_{\phi a}$. Once we achieve this result, it should be obvious from the above discussion that we have reached a local, if not global, minimum of the overall phase-noise response of a particular oscillator circuit.

There are at least two pertinent open questions which are obvious at this juncture. First, what are the design rules for minimizing $D_{\phi a}$, i.e., what topologies and parameter settings induce optimal performance, and second, are the special states, $D_{\phi a} = 0$, referred to here as the *zero-states*, attainable at all.

In Djurhuus and Krozer,[13] using a novel model framework based on the concept of oscillator conjugacy, the authors were able to answer both these questions for the special case of two-dimensional oscillators. There it was proven that zero-states were predicated on a symmetric oscillator limit-cycle solution. Hence, we have the situation : $D_{\phi a} = 0 \Rightarrow$ symmetric steady-state. This novel and wide-reaching result has many direct implications for practical oscillator design. Most importantly, it clearly identifies the zero-states ($D_{\phi a} = 0$) in the oscillator solution space. Knowing the zeros of a measure is an absolute requirement for the development of optimization algorithms which hitherto were not possible. In the following, we shall refer to the model framework developed in Djurhuus and Krozer[13] as the SYM-AM/PM model.

Several numerical experiments, performed in both Djurhuus and Krozer[13] and in this paper, unequivocally verify all the predictions put forth by the novel SYM-AM/PM model. However, these simulations also indicate that zero-states remain generally unattainable for many industry-standard radiofrequency (RF) and μ-wave oscillators circuit topologies. In fact, our work shows that these circuit-classes only achieve zero-states in special limit-cases which are of no significant value for practical design. Herein, we refer to these solution points as *ambiguous zero-states* or A-STATE(S) for short. The prevalence of A-STATES in industry-standard oscillator circuits is certainly an unsatisfying situation. In this paper, we intend to remedy this situation by applying the design rules acquired from the application of the novel SYM-AM/PM model. Specifically, we demonstrate the synthesis of a novel LC oscillator circuit which achieves zero-states ($D_{\phi a} = 0$) while operating at realistic output-power levels. These kinds of zero-states, with real prospects for design value, will be referred to as *proper zero-states* or P-STATE(S) for short. This exercise will clearly illustrate how the SYM-AM/PM model framework can be applied towards synthesis and design of optimized oscillator solutions. Furthermore, this exercise will highlight how this theoretical program can be used to develop novel numerical algorithms aimed at optimizing oscillator phase-noise performance.

The paper is organized in six sections. Section 2 delivers a comprehensive review of the main theoretical concepts involved. Then, in Section 3, we introduce the SYM-AM/PM model, which was developed in Djurhuus and Krozer,[13] review the various predictions which follow from its use and announce the various numerical measures to be used in subsequent simulations. Section 4 contains numerical experiments on a MOSFET transistor differential-pair LC oscillator circuit, a very important unit found in most modern RF and μ-wave systems. The simulations unequivocally verify all the predictions emerging from the SYM-AM/PM model. Section 5 details the synthesis and simulation of the novel SYM-OSC oscillator circuit. It is shown that the SYM-OSC attains zero-states for parameter settings allowing the oscillator to operate at realistic output power levels, so-called P-STATES. Finally, Section 6 gives a brief discussion of the obtained results and future work which we plan to pursue.

2 | A BRIEF REVIEW OF ESTABLISHED THEORY

We consider an n-dimensional autonomous vector-field $f : \mathbb{R}^n \to \mathbb{R}^n$ generating a set of n-coupled ordinary differential equations (ODEs)

$$\dot{x} = f(x) \tag{1}$$

with $x(t) : \mathbb{R} \to \mathbb{R}^n$ being the n-dimensional time-dependent state-vector. The dynamical system in Equation (1) produces a stable limit set γ known as the oscillator *limit-cycle*. A steady-state solution $x_s(t+T) = x_s(T)$ is a T-periodic

solution orbit with an initial condition in γ. It then follows that $x_s(\tau) \in \gamma$ for all τ. The system in Equation (1) is time-normalized using the timescale $\tau = 2\pi(t/T)$ which implies a 2π periodic solution $x_s(\tau + 2\pi) = x_s(\tau)$ and corresponding oscillator frequency $\omega_0 = 2\pi/T = 1$.

2.1 | Linear response map Φ and the oscillator tangent bundle $\mathbb{TR}^n$

The oscillator response, $\delta x(\tau)$, to small perturbations around the steady-state, $\gamma(\tau)$, is governed by the oscillator *linear-response* map $\Phi(q,s) : \mathbb{T}_s\mathbb{R}^n \to \mathbb{T}_q\mathbb{R}^n$. This map produces the oscillator output $\delta x(q) = \Phi(q,s)\zeta(s)$, at time $\tau = q$, in response to a small (deterministic or random/noise) perturbation vector $\zeta(s)$, at time $\tau = s$. Here, the oscillator *tangent space* $\mathbb{T}_\eta\mathbb{R}^n$ represents the usual real n-dimensional vector-space $\mathbb{R}^n$ with the origin translated to the point $\gamma(\eta)$ in state-space (an *affine* vector-space). The entire domain and co-domain (image) of the map Φ, $\mathbb{TR}^n$, is known as the oscillator *tangent-bundle*, is then given as union of the individual tangent spaces

$$\mathbb{TR}^n = \bigcup_{\eta \in [0;2\pi[} \mathbb{T}_\eta\mathbb{R}^n. \tag{2}$$

2.2 | The Floquet decomposition

For hyperbolic stable oscillators, the following unique decomposition of Φ will always exist:

$$\Phi(q,s) = \sum_{k=1}^{n} \exp(-\mu_k(q-s)) u_k(q) v_k^\dagger(s), \tag{3}$$

where $\{\mu_i\}$ are the n characteristic Floquet exponents, $\{u_i(\tau)\}$ is the complete set of Floquet vectors, and $\{v_i(\tau)\}$ is the complete set of *dual*[*] Floquet vectors.[10-12]

The Floquet vectors and dual vectors support the following defining relationship:

$$v_i^\dagger(\tau_a) u_j(\tau_b) = \delta(\tau_a - \tau_b)\delta_{ij} \text{ for} i = 1, 2, ...n, \tag{4}$$

where $v_i^\dagger$ denotes the transposed of the (dual) vector v_i, δ_{ij} is the Kroenecker delta-function, whereas τ_a, τ_b are two normalized time-points. The delta-function component of Equation (4) signifies that the bi-orthogonality property only holds for equal time arguments. The set $\{u_i(\tau)\}$ is complete, and we can hence always decompose any perturbation vector function as

$$\zeta(\tau) = a_1(\tau)u_1(\tau) + a_2(\tau)u_2(\tau) + ... + a_n(\tau)u_n(\tau), \tag{5}$$

where $\{a_i(\tau)\}$ are n expansion coefficient functions. From Equation (4), one then finds directly

$$v_k^\dagger(\tau)\zeta(\tau) = a_k(\tau), \tag{6}$$

and the dual vector v_k hence picks out the component of ζ proportional to u_k.

For an autonomous oscillator solution, the special exponent $\mu_1 = 0$ will always occur. The corresponding Floquet vector u_1, known as the *phase-mode*, is a scaled version of $\dot{x}_s$, where x_s is the steady-state solution of the system in

*The difference between vectors and dual vectors is that they transform as contra-variant and co-variant vectors, respectively.[11] Henceforth, the terms *vector* and *vector-bundles* are thus connected to contra-variant vectors and vector-functions, whereas the terms *dual vector* and *dual vector-bundles* are associated with co-variant vectors and vector-functions.

Equation (1) and hence tangent to the limit-cycle γ.[10,11] Setting $k=1$ in Equation (6), it follows that the dual-vector $v_k = v_1$ collects the part of the perturbation attributed to phase-mode $u_k = u_1$ as seen from Equation (5). When ζ is a noise perturbation, it thus collects the oscillator *phase-noise* contribution. The dual vector, v_1, hence has special status as it relates to the oscillator phase-response and is often referred to in the literature as the perturbation-projection vector (PPV).[10] For an autonomous oscillator, all that is not phase must, by definition, be amplitude. Hence, the remaining $n-1$ Floquet vectors $\{u_i(\tau)\}_{i=2}^{n}$ are referred to as *amplitude-modes* and stability requires $\Re\{\mu_{(i>1)}\} < 0$, where $\Re\{\mu_i\}$ denotes the real part of the complex coefficient μ_i.

The n Floquet vector functions $\{u_i(\tau)\}$ are now grouped in two so-called *vector-bundles*[11]

$$\mathbb{TM} = \text{span}\{u_1(\tau)\}, \tag{7}$$

$$\mathbb{TI} = \text{span}\{u_2(\tau), u_3(\tau), ..., u_n(\tau)\} \tag{8}$$

with $\mathbb{TM}$ containing the single phase-mode, whereas the bundle $\mathbb{TI}$ holds the $n-1$ amplitude-modes. The oscillator tangent-bundle in Equation (2) can then be decomposed into phase and amplitude contributions as

$$\mathbb{TR}^n = \mathbb{TM} \oplus \mathbb{TI}, \tag{9}$$

The bundle definitions in Equation (7)–(8) then prompt the definition of the equivalent dual bundles (see footnote *)

$$\mathbb{T}^*\mathbb{M} = \text{span}\{v_1(\tau)\}, \tag{10}$$

$$\mathbb{NM} = \text{span}\{v_2(\tau), v_3(\tau), ..., v_n(\tau)\}. \tag{11}$$

The geometric interpretation behind the concepts discussed above are illustrated qualitatively in Figure 1A. For a more thorough discussion of these topics, we refer to Djurhuus et al.[11]

2.3 | The orthogonal decomposition of $\mathbb{TR}^n$

We consider the scenario where the phase-mode, u_1, and the PPV, v_1, are colinear $u_1(\tau) = a v_1(\tau)$, $a \in \mathbb{R}$. From Equations (7) and (10), we then have[†] $\mathbb{TM} \simeq \mathbb{T}^*\mathbb{M}$. From the rule in Equation (4) and the definition of $\mathbb{TI}$ in Equation (8), it follows that v_1 is always orthogonal to $\mathbb{TI}$ and since u_1 and v_1 are colinear, it follows that u_1 now also must be orthogonal to $\mathbb{TI}$. By definition, u_1 is orthogonal to the dual space $\mathbb{NM}$ defined in Equation (11), and we therefore must have $\mathbb{TI} \simeq \mathbb{NM}$. We sum up the above discussion as

$$\mathbb{TM} \simeq \mathbb{T}^*\mathbb{M} \Leftrightarrow \mathbb{TI} \perp \mathbb{TM}, \tag{12}$$

where $Q \perp W$ implies that the bundles Q and W are orthogonal. This *orthogonal decomposition* scenario is illustrated qualitatively in Figure 1B.

2.4 | The oscillator phase-noise spectrum

In this section, we consider the noise-perturbed version of the oscillator defined in Equation (1)

$$\dot{x} = f(x) + b(x)z(\tau), \tag{13}$$

[†]Here, we use the notation $\mathbb{X} \simeq \mathbb{Y}$ to indicate that the vector-bundle (contra-variant bundle) $\mathbb{X}$ and the dual bundle (co-variant bundle) $\mathbb{Y}$ describe the same subspace of $\mathbb{TR}^n$ (see footnote *).

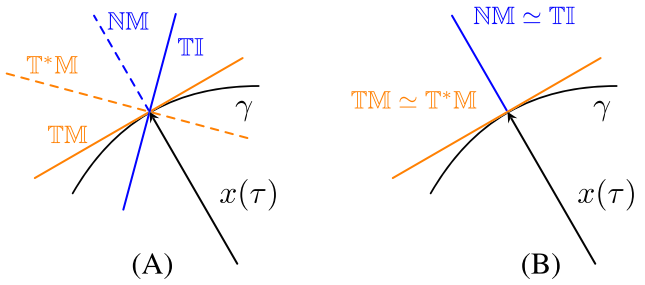

FIGURE 1 (A) A qualitative picture illustrating the Floquet vector-bundles $\mathbb{TM}, \mathbb{TI}$ (solid line) and the dual vector-bundles $\mathbb{T}^*\mathbb{M}, \mathbb{NM}$ (dashed line). (B) W hen vector u_1 and dual vector v_1 are colinear, i.e., $u_1 = av_1$, $a \in \mathbb{R}$, we attain the orthogonal decomposition $\mathbb{TM} \perp \mathbb{TI}$ [Colour figure can be viewed at wileyonlinelibrary.com]

where $b : \mathbb{R}^n \to \mathbb{R}^{n\times p}$ is the noise modulation matrix[10] and $z : \mathbb{R} \to \mathbb{R}^p$ is a p-dimensional vector of uncorrelated, zero-mean, unit-power Gaussian white noise sources[‡]. Note that since the noise analysis herein is based on the linear-response (see discussion in Sections 2.1–2.2), the model implicitly assumes that the power of the noise sources z_k are weak compared to the deterministic signals $x = (x_1, x_2, ...x_n)^\dagger$. Specifically, this is the situation for the important case of electrical oscillators operating at room temperature. The noise perturbation in Equation (13), evaluated on the oscillator steady-state solution $x_s(\tau)$, can now be written

$$\xi(\tau) = b(x_s(\tau))z(\tau) = \sum_{k=1}^{p} b_k(\tau)z_k(\tau), \tag{14}$$

where $b_k(\tau)$ is the kth column of the modulation matrix $b(x(\tau))$, whereas $z_k(\tau)$ is the kth component of the noise-vector z.

As the p noise sources $\{z_k(\tau)\}$ in Equation (14) are uncorrelated, and equally distributed (i.e., white Gaussian noise), the total response of any ensemble average function (such as diffusion constants) can found by adding the individual contributions using the superposition principle. We can hence simplify the notation of the following analysis significantly by only considering the response of the oscillator to a single noise source. Hence, let $1 \le q \le p$ and consider the qth term in Equation (14). We then define the simplified perturbation source as

$$\xi(\tau) = \kappa(\tau)s(\tau), \tag{15}$$

where $\kappa(\tau) = b_q(\tau)$ and $s(\tau) = z_q(\tau)$. In the following analysis, the various calculations are performed using the source in Equation (15) as the oscillator noise perturbation. Later in the analysis phase, the superposition principle will then be applied to show how this partial, single-source, response actually directly implies the total oscillator response produced by the full perturbation vector in Equation (14).

From the discussion in Section 2.2, and the expression of the Φ in Equation (3), we know that the dual Floquet vector v_1 (PPV) collects all noise perturbations attributed to the phase-mode u_1, i.e., phase-noise. Specifically, given the noise perturbation vector ξ, the so-called oscillator *phase-diffusion* D is calculated as

$$D = \frac{1}{2\pi}\int_0^{2\pi} v_1^\dagger(s)\langle\xi(s)\xi^\dagger(s)\rangle v_1(s)ds, \tag{16}$$

The oscillator phase-noise spectrum, around the first harmonic (carrier), then takes the (time-normalized) form[10-12]

$$\mathfrak{L}(f_m) = 10\log\left(\frac{4D}{D^2 + 4f_m^2}\right), \tag{17}$$

[‡]Note that the power of the time-normalized noise sources in Equation (13) is scaled by a factor $2\pi/T$ compared to the original un-normalized sources, as a simple calculation would reveal. The results discussed herein are independent of time-normalization, and this scale factor hence is not critical for our investigation. It is therefore simply absorbed in modulation matrix b.

where f_m is the normalized offset-frequency from the carrier. The model leading to spectrum in Equation (17) assumes a stable carrier which is an acceptable approximation for most practical electrical oscillator circuits, at least for reasonable time-scales. However, it should be mentioned that this approach does neglect thermal and noise-induced drift of the carrier frequency. For a more detailed description of the stochastic oscillator phase process, including drift, we refer to the literature.[14-17]

We now decompose the phase-diffusion in Equation (16) into two separate contributions

$$D = \underbrace{D_{\phi\phi}}_{\text{PM-PM}} + \underbrace{D_{\phi a}}_{\text{AM-PM}}, \tag{18}$$

where $D_{\phi\phi}$ represents the part of the phase-diffusion due to PM noise (noise tangent to γ) and $D_{\phi a}$ represent the component due to AM noise (noise orthogonal to γ), i.e., the AM-PM noise conversion. The calculation of these parameters is the topic of the following section.

2.5 | AM-PM noise conversion

We consider the vector-bundle $\mathbb{N}^*\mathbb{M} \simeq \mathbb{N}\mathbb{M}$

$$\mathbb{N}^*\mathbb{M} = \text{span}\{\hat{a}_1(\tau), \hat{a}_2(\tau), \ldots, \hat{a}_{n-1}(\tau)\}, \tag{19}$$

which is simply just the contra-variant version of the dual vector-bundle $\mathbb{N}\mathbb{M}$ in Equations (11) (see footnotes * and †). Together with the unit vector bundle $\phi(\tau) \in \mathbb{T}\mathbb{M}$, we can construct the orthonormal frame $(\hat{\phi}, \{\hat{a}_i\})$ shown in Figure 2. From this frame, the noise vector $\xi(\tau)$ in Equation (15) is decomposed into phase (PM) and amplitude (AM) components

$$\xi(\tau) = \underbrace{\alpha_0(\tau)\hat{\phi}(\tau)s(\tau)}_{\text{PM noise}} + \sum_{k=1}^{n-1} \underbrace{\alpha_i(\tau)\hat{a}_i(\tau)s(\tau)}_{\text{AM noise}}, \tag{20}$$

where $\alpha_0(\tau) = \kappa^\dagger(\tau)\hat{\phi}(\tau)$, $\alpha_{i>0}(\tau) = \kappa^\dagger(\tau)\hat{a}_i(\tau)$. The following projections are now defined

$$v_1^\dagger(\tau)\hat{\phi}(\tau) = \beta_0(\tau), \tag{21}$$

$$v_1^\dagger(\tau)\hat{a}_i(\tau) = \beta_i(\tau), \tag{22}$$

where v_1 is the dual phase-mode Floquet vector (PPV) discussed in Section 2.2. From Equation (6), it follows that the $\mathbb{T}\mathbb{M} = \text{span}(u_1(\tau))$ component of any arbitrary vector x is calculated from the projections $v_1^\dagger(\tau)x$. Furthermore, if we define $y = x - v_1^\dagger(\tau)x$, then, it must follow that $y \in \mathbb{T}\mathbb{I}$; as $v_1^\dagger(\tau)y = 0$ (see discussion in Section 2.2). Using the definition of $\mathbb{T}\mathbb{I}$ in Equation (8) and the projections in Equations (21)–(22), we can then write the noise vector in Equation (20) as

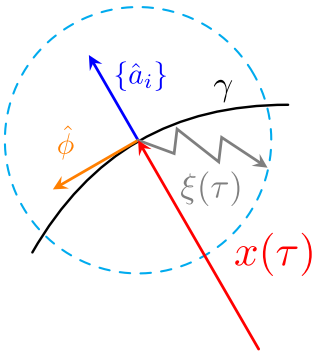

FIGURE 2 The noise vector ξ, defined in Equation (15), is decomposed into phase (PM) and amplitude (AM) components according to the orthonormal frame $(\hat{\phi}, \{\hat{a}_i(\tau)\})$ [Colour figure can be viewed at wileyonlinelibrary.com]

$$\xi(\tau) = [\underbrace{\rho(\tau)}_{\text{PM-PM}} + \underbrace{\lambda(\tau)}_{\text{AM-PM}}]u_1(\tau)s(\tau) + \sum_{k=2}^{n}\nu_{k-1}(\tau)u_k(\tau)s(\tau), \tag{23}$$

where $\{\nu_k(\tau)\}$ are a set of $n-1$ unspecified functions representing the oscillator amplitude-noise response, whereas $\rho, \lambda : \mathbb{R} \to \mathbb{R}$ are two real functions, representing the PM/AM-noise contributions to the phase mode u_1. From this description, it follows that ρ holds the phase-mode (u_1) noise component due to PM noise (PM-PM), whereas λ holds the phase-mode noise component due to AM noise (AM-PM). From Equations (20) and (21)–(22), these two functions are written

$$\rho(\tau) = \alpha_0(\tau)\beta_0(\tau), \tag{24}$$

$$\lambda(\tau) = \sum_{i=1}^{n-1}\alpha_i(\tau)\beta_i(\tau). \tag{25}$$

The following statement explains under what circumstances the AM-PM contribution in Equation (23), $\lambda(\tau)$, can be zero

Corollary 2.1. The function $\lambda : \mathbb{R} \to \mathbb{R}$ defined in Equation (25) will be zero if, and only if, the Floquet decomposition is orthogonal (see Section 2.3 and Figure 1)

$$\lambda(\tau) = 0 \Leftrightarrow \mathbb{TM} \perp \mathbb{TI}. \tag{26}$$

Proof. From Equations (25) and (22)

$$\lambda(\tau) = 0 \Leftrightarrow \sum_{i=1}^{n-1}\alpha_i(\tau)\beta_i(\tau) = \sum_{i=1}^{n-1}\alpha_i(\tau)v_1^{\dagger}(\tau)\hat{a}_i(\tau) = v_1^{\dagger}(\tau)w(\tau) = 0, \tag{27}$$

where $w(\tau) = \sum_{i=1}^{n-1}\alpha_i(\tau)\hat{a}_i(\tau)$. The frame $\{\hat{a}_i\}$, shown in Figure 2, spans the normal-space $\mathbb{N}^*\mathbb{M} \simeq \mathbb{NM}$ which implies $w(\tau) \in \mathbb{N}^*\mathbb{M}$. This frame is orthogonal to the limit cycle γ (see Figure 2). As $w(\tau) \in \mathbb{N}^*\mathbb{M}$, Equation (27) then implies that v_1 is orthogonal to $\mathbb{N}^*\mathbb{M} \simeq \mathbb{NM}$ which means that it must be tangent to γ (see Figure 1). The vectors v_1 and u_1 are hence colinear, *i.e.,* $\mathbb{TM} \simeq \mathbb{T}^*\mathbb{M}$ (see Section 2.3). But then it follows directly from Equation (12) that the Floquet decomposition must be orthogonal.

We proceed with the statement

Corollary 2.2. Given the decomposition of ξ in Equation (23) and the definition of the AM-PM phase-diffusion constant $D_{\phi a}$ in Equation (18), we have

$$\lambda(\tau) = 0 \Leftrightarrow D_{\phi a} = 0, \tag{28}$$

where the function $\lambda : \mathbb{R} \mapsto \mathbb{R}$ is defined in Equation (23).

Proof. See Appendix C1.

At this point, we must remind ourselves that the above results were derived using the single source $\kappa(\tau)s(\tau) = b_q(\tau)z_q(\tau)$ in Equation (15) which represented the qth component of the sum in Equation (14). Hence, from this point on, the notation $D_{\phi a}^{(q)}$ is used to refer to the partial AM-PM phase-diffusion constant due to the perturbation $b_q(\tau)z_q(\tau)$, whereas $D_{\phi a}$ is now reserved for the response due to the full noise perturbation in Equation (14). Combining the results in corollaries 2.1 and 2.2, then gives the result

$$D_{\phi a}^{(q)} = 0 \Leftrightarrow \mathbb{TM} \perp \mathbb{TI}. \tag{29}$$

As mentioned above, the superposition principle can be applied to tie the partial result in Equation (29) to full response. For this purpose, we now state

Corollary 2.3. The partial result in Equation (29), calculated using the single source in Equation (15), holds equally for the response due to the full perturbation vector in Equation (14)

$$D_{\phi a} = 0 \Leftrightarrow \mathbb{TM} \perp \mathbb{TI}, \tag{30}$$

where, as mentioned above, $D_{\phi a}$ now refers to the full AM-PM phase-diffusion constant calculated using $\xi(\tau)$ in Equation (14).

Proof. Repeating the above calculation for each term $b_k(\tau)z_k(\tau)$ in Equation (14), we would again arrive at Equation (29) for $q = k$. Since the sources $z_k(\tau)$ are uncorrelated, the ensemble averages will not contain any cross-terms meaning that the response of each of the terms are mutually independent. It then follows directly from the superposition principle that the full AM-PM phase-diffusion constant is given as the sum $D_{\phi a} = \sum_{k=1}^{p} D_{\phi a}^{(k)}$. Furthermore, as a diffusion constant cannot be negative, we have

$$D_{\phi a} = \sum\nolimits_{k=1}^{p} D_{\phi a}^{(k)} = 0 \Leftrightarrow D_{\phi a}^{(x)} = 0 \text{ for } x = 1, 2, \ldots p, \tag{31}$$

which says that $D_{\phi a}$ is zero if, and only if, all the partial terms $\{D_{\phi a}^{(q)}\}$ are zero. Each term in this sum obeys Equation (29), and combining this result with Equation (31), one arrives directly at Equation (30).

As discussed in Section 1, we refer to $D_{\phi a} = 0$ (zero AM-PM noise conversion) as *zero-states*. Equation (30) then says that zero-states are only possible if the Floquet decomposition is orthogonal, i.e., $\mathbb{TI} \perp \mathbb{TM}$. Using the definitions of $\mathbb{TM}$ and $\mathbb{TI}$ in Equations (7) and (8), this translates directly to the following condition for the special two-dimensional ($n = 2$) case

$$D_{\phi a} = 0 \Leftrightarrow u_1(\tau) \perp \mathrm{u}_2(\tau). \tag{32}$$

Hence, in-order for a two-dimensional oscillator to attain a zero-state, we must demand that the corresponding Floquet phase and amplitude-modes, $u_1(\tau)$ and $u_2(\tau)$, are orthogonal for all values of τ.

3 | THE SYM-AM/PM MODEL

In[13] a new methodology, based on the concept of oscillator conjugacy, was developed with the aim of analyzing oscillator noise response. In this text, we refer to this theoretical framework as the SYM-AM/PM model.

One prominent and wide-reaching prediction which emerges from the SYM-AM/PM model is represented by the following statement[13]:

$$u_1(\tau) \perp \mathrm{u}_2(\tau) \Rightarrow \gamma \in \mathbb{S}_{\mathrm{a}}, \tag{33}$$

where $\mathbb{S}_a$ is the collection of rotationally symmetric limit sets

$$\mathbb{S}_a = \{w \in \mathbb{W}_s \,|\, |w| - |a| = 0\}\ a \in \mathbb{C}, \tag{34}$$

with $\mathbb{W}_s$ being the 2-D oscillator stable manifold[§] which is indexed here using the complex coordinate w. Note that $\mathbb{S}_a$ simply holds all limit-sets which have the form of concentric circles centered at the point a. In words, Equations

[§]As explained in Djurhuus and Krozer,[13] the stable manifold $\mathbb{W}_s$ must be diffeomorphic to the punctured plane $\mathbb{C}\backslash\{0\}$. However, this just says that the oscillation must bifurcate from a single DC operating point. Fortunately, this definition covers all practically useable electrical oscillator topologies as well as almost all mathematical examples such as the van-der-Pol circuit class and the Selkov model.

(33)–(34) say that an orthogonal decomposition is achieved if, and only if, the underlying steady-state oscillator solution $\gamma(\tau)$ is perfectly symmetric. This connection between γ-symmetry and an orthogonal Floquet decomposition was first discovered in Djurhuus and Krozer.[13]

Combining the result in Equation (33) with Equation (32), calculated in the previous section, we arrive at the novel statement

$$D_{\phi a} = 0 \Rightarrow \gamma \in \mathbb{S}_a, \tag{35}$$

which says essentially that for 2-D oscillators, zero AM-PM noise conversion follow from the symmetry of the steady-state (deterministic) oscillator solution.

In-order to numerically test and verify the novel hypothesis in Equation (35), we will need to quantify the levels of γ-symmetry and AM-PM noise conversion. For this purpose, we introduce the measure

$$\Lambda = \left| \frac{1}{2\pi} \int_0^{2\pi} \{(\rho(\tau)/\rho_{\max}) - 1.0\} d\tau \right|, \tag{36}$$

where $\rho(\tau) = |\gamma(\tau)|^2 = \gamma_1(\tau)^2 + \gamma_2(\tau)^2$, with $\gamma_{1,2}$ being the two components of the 2-D limit-cycle solution $(\gamma(\tau) = (\gamma_1(\tau), \gamma_2(\tau)))$, whereas $\rho_{\max}$ representing the maximal value of the function ρ on the interval $\tau \in [0; 2\pi]$. From the definition of $\mathbb{S}_a$ in Equation (34) and the expression above, it should be clear that $\Lambda = 0 \Leftrightarrow \gamma \in \mathbb{S}_a$ and Λ hence measures the level of limit-cycle symmetry, with $\Lambda = 0$ for a perfectly symmetric solution. Next, we consider the function

$$\Upsilon = \max_{\tau \in [0;2\pi]} |\angle\{\mathrm{u}_1(\tau), \mathrm{u}_2(\tau)\} - 90^\circ|, \tag{37}$$

where $u_{1,2}(\tau)$ are the first and second Floquet vector functions, respectively. It follows directly from Equation (32) that Υ measures the level of AM-PM in the solution, with $\Upsilon = 0$ representing the zero-states discussed above. Using the definitions in Equation (36)–(37), it follows that in order for Equation (33), and consequently Equation (35), to hold true, we must observe

$$\Upsilon \to 0 \Rightarrow \Lambda \to 0, \tag{38}$$

in our numerical simulation results.

The predictions which emerge from the SYM-AM/PM model directs us to seek out oscillator topologies and parameter settings which produce the symmetric ($\Lambda = 0$) steady-state solution, contained in the set $\mathbb{S}_a$ in Equation (34), in order to achieve oscillators operating at the zero-states ($\Upsilon = 0$). Unfortunately, as will be discussed below, these $\Lambda = 0$ states seem to generally not occur in industry-standard RF and μ-wave oscillator circuit topologies. In fact, as will be made evident in subsequent simulation trials, these circuit-classes only attain zero-states in special limit-cases which are unworkable from a practical design perspective, the so-called A-STATES. The issues discussed here will become more accessible in the following section where we consider a reduced-order model of a specific MOSFET transistor differential-pair cross-coupled oscillator which is a unit found in many modern communication and remote-sensing applications. This state-of-affairs will prompt us in Section 5 to demonstrate the synthesis of a novel 2-D LC oscillator circuit, constructed using the design rules newly acquired from the SYM-AM/PM model, which in fact does present several practically useful zero-states, the so-called P-STATES.

4 | A STANDARD MOSFET TRANSISTOR OSCILLATOR CIRCUIT—AMBIGUOUS ZERO-STATES (A-STATES)

We consider the MOSFET differential pair LC oscillator, shown in Figure 3A. Here, we consider both the series resonator load (red) and parallel resonator load (blue) options. The circuit operates in the *current-limited* regime[18] implying that the NMOS differential pair behaves as an ideal switch. From Figure 3A, the circuit is biased by the DC current source I_B and the small-signal transconductance is then written

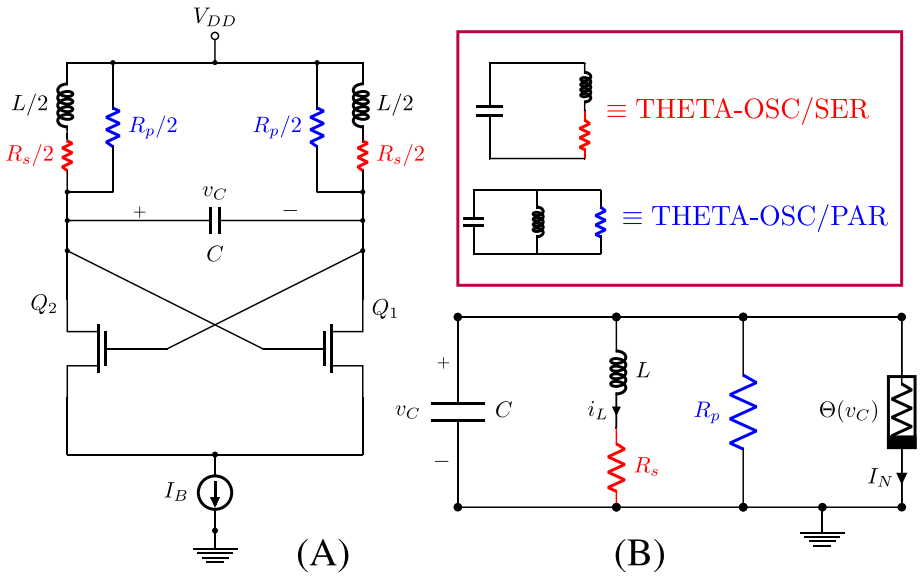

FIGURE 3 (A) A cross-coupled MOSFET (NMOS) LC oscillator operating in the current-limited regime. (B) The equivalent 2-D circuit for the differential-mode oscillation, THETA-OSC, where the nonlinear transconductance Θ models the MOSFET pair in figure A). The circuit includes either a series (THETA-OSC/SER) or parallel (THETA-OSC/PAR) resonator load [Colour figure can be viewed at wileyonlinelibrary.com]

$$G_m = \sqrt{k_n I_B}, \tag{39}$$

where $k_n = \mu_n C_{\text{ox}} W_n / L_n$ with μ_n, C_{ox}, W_n, and L_n being the charge mobility, oxide capacitance, gate width, and length, respectively. Using the result in Equation (39), the full nonlinear transconductance function of the MOSFET differential pair in Figure 3A is then approximated[19]

$$\Theta(v_C) = I_B \frac{2}{\pi} \arctan\left(\frac{\pi}{2} \frac{G_m}{I_B} v_C\right), \tag{40}$$

where v_C is the resonator differential capacitor voltage (see Figure 3). In Figure 3B, the differential-mode equivalent of the full transistor circuit, referred to as the THETA-OSC, is shown. We consider both the series resonator load THETA-OSC/SER (red) and parallel resonator load THETA-OSC/PAR (blue) options. In the following, we normalize the time variable as $\tau = \omega_n t$ where $\omega_n = 1.0/\sqrt{LC}$ is the natural frequency of the resonator. The dynamical equations of the 2-D differential-mode THETA-OSC reduced-order circuit are then written as

$$\begin{aligned} \dot{x} &= -(z_0/R_p)x - y/z_0 + \Theta(z_0 x) \\ \dot{y} &= z_0 x - (R_s/z_0)y, \end{aligned} \tag{41}$$

with $x = v_C/z_0$, $y = i_L z_0$, where v_C, i_L are the voltage across the capacitor C and current through inductor L, respectively, whereas $z_0 = \sqrt{L/C}$ is the resonator characteristic impedance and Θ was defined above in Equations (39)–(40) [¶]. Here, $R_p, R_s \neq 0$ corresponds to the THETA-OSC/[PAR/SER] circuits in Figure 3 with corresponding color codes (blue/red). The capacitance C and inductance L do not occur explicitly in Equation (41) but are easily calculated from the given parameters[#].

Figure 4A shows a series of numerical calculations for the THETA-OSC/PAR circuit in Figure 3B as modeled by Equation (41) (blue). We consider a constant Q circuit with $Q = 10$ corresponding to a resonator load $R_p = Q/(\omega_n C) = Q z_0$. The figure plots the two measures Υ, Λ in Equations (37) and (36) as function of the bias current I_B (see Figure 3A) and for four values of the resonator characteristic impedance z_0. In Figure 4A, the concept of an

[¶]In the following, we fix k_n from Equation (39), in time-scaled form, as $k_n = 2AV^{-2}$.

[#]As the resonator natural frequency $\omega_n = 1.0/\sqrt{LC}$ is fixed (time normalization), we can express the circuit capacitance and inductance in terms of parameters ω_n, z_0 as $C = 1.0/(\omega_n z_0)$ and $L = z_0/\omega_n$.

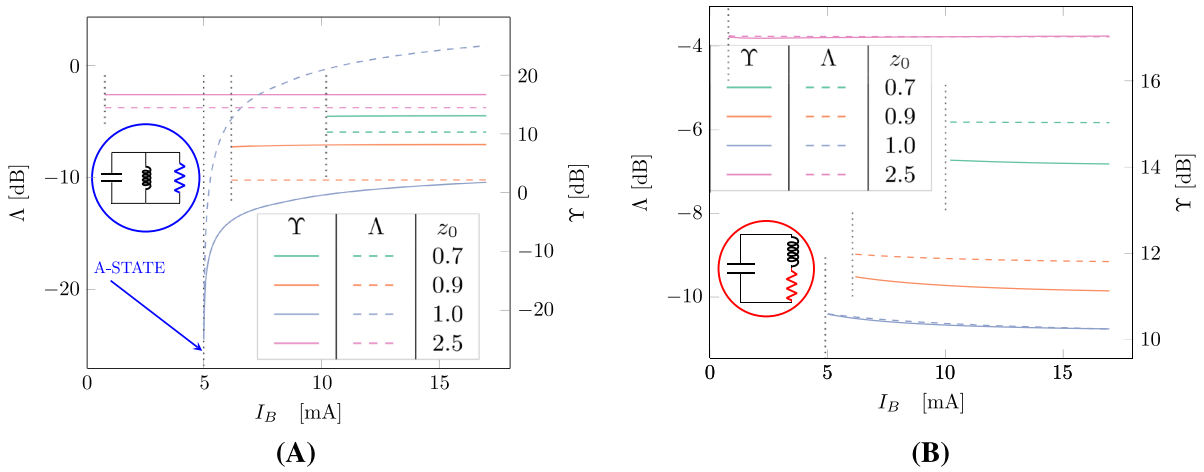

FIGURE 4 Simulations of measures Υ and Λ, defined in Equations (37) and (36), for THETA-OSC differential-mode circuit (see Figure 3B). (A) parallel load, THETA-OSC/PAR (blue), Q-factor : $Q = 10$, dotted lines = SB in Equation (42). (B) Series load THETA-OSC/SER (red), Q-factor : $Q = 10$, dotted lines = SB in Equation (43) [Colour figure can be viewed at wileyonlinelibrary.com]

oscillator *start-up boundary* (SB) is introduced. Herein, the term SB represents the point in parameter space where the oscillator solution is born, i.e., starts-up, from the DC operating point in some-kind of bifurcation (Hopf-bifurcation in our case). The THETA-OSC/PAR circuit starts-up (turns-on) at $G_m > G_{m0} = 1.0/R_p = 1.0/(Qz_0)$. Using the relation in Equation (39), we can then find the bias current I_{B0} at start-up

$$I_{B0} = 1.0/(k_n Q^2 z_0^2). \tag{42}$$

Here, I_{B0} describes the SB as for $I_B < I_{B0}$, the system is at rest (i.e., DC rest point) and for $I_B > I_{B0}$, the dynamics of the system is described by a periodic limit-cycle solution. The boundary $I_B = I_{B0}$ hence represents the transition between these two states (i.e., the bifurcation point). The four SBs, one for each value of z_0, in Equation (42), are indicated in the figure as dotted vertical lines. We note that $\Lambda, \Upsilon \to 0$ as $I_B \to I_{B0}$ exclusively for the parameter value $z_0 = 1.0$. Each curve in Figure 4A corresponds to a unique set of circuit resonator parameters (C, L, R_p) as explained in footnote # and the above derivation of the parallel load as $R_p = Qz_0$.

Figure 4B repeats the experiments displayed in Figure 4A above but this time for the THETA-OSC/SER circuit (see Figure 3B [red]) modeled by Equation (41) (red). Here, the resonator quality factor Q is again fixed as $Q = 10$ corresponding to a resonator load $R_s = \omega_n L/Q = z_0/Q$. A simple series-to-parallel transformation then gives the following approximation for the equivalent parallel load $\hat{R}_p \approx R_s(1 + Q^2)$. From the discussion above, we know that the oscillator circuit turns on for $G_m > G_{m0} = 1.0/\hat{R}_p = (Q/z_0)/(1 + Q^2)$. Using Equation (39) results in the following approximate values for the SBs for the TANH-OSC/SER circuit in Figure 3B,

$$I_{B0} \approx (Q/z_0)^2/\left(k_n\left[1 + Q^2\right]^2\right), \tag{43}$$

which depend on the value of the characteristic impedance z_0, and are indicated in Figure 4B using vertical dotted lines. Unlike what was observed in Figure 4A, no singularities, for either measure, occur for the TANH-OSC/SER at the SBs. Each curve in Figure 4B corresponds to a unique set of circuit resonator parameters (C, L, R_s) as explained in footnote # and the above derivation of the series load as $R_s = z_0/Q$.

Figure 4A, which represents simulation results for the THETA-OSC/PAR circuit, featured a singularity in both measures Λ and Υ, at the SB, for the parameter setting $z_0 = 1$. Furthermore, this singularity occurred strictly pairwise, by which is meant that is was never the case that $\Upsilon \to 0$ while $\Lambda \not\to 0$ for any parameter setting. From the above description, it follows that the THETA-OSC/PAR circuit has a *zero-state* (i.e., $\Upsilon = 0$) at the SB. In contrast, the numerical experiments in Figure 4B, for the THETA-OSC/SER circuit, showed no evidence of singularities. While the THETA-OSC/SER again attains minimum AM-PM, as measured by Υ, for $z_0 = 1.0$, it never achieves any zero-states at the SB

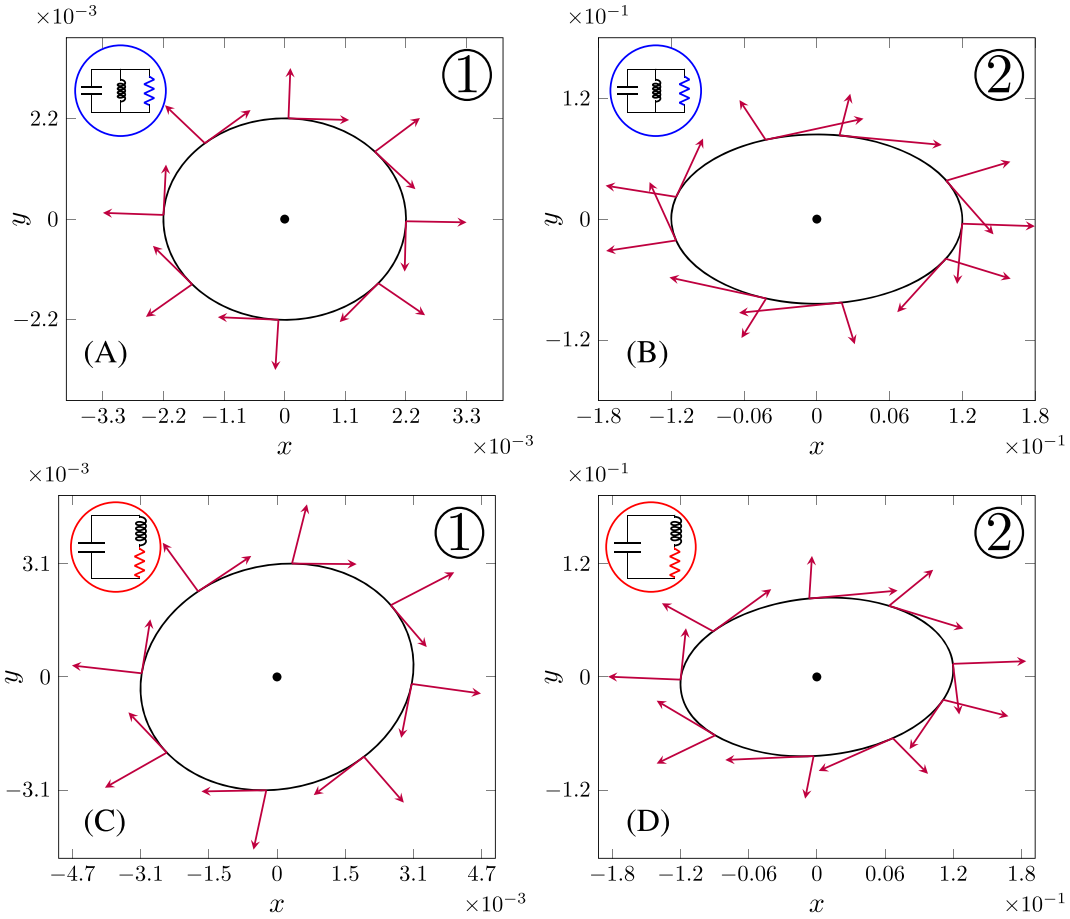

FIGURE 5 Plots of four limit-cycle solutions and corresponding Floquet vector-bundle for the THETA-OSC circuit in Figure 3. The two figures on the left and right column correspond to simulations for the parameter settings ① : $(I_b, z_0) = (\sim 5.0mA, 1.0\Omega)$ and ② : $(I_b, z_0) = (15.0\text{mA}, 0.7\Omega)$, respectively. The two figures on the top and bottom row of the matrix correspond to plots for the THETA-OSC/[PAR/SER] circuits ((blue/red) in Figure 3) [Colour figure can be viewed at wileyonlinelibrary.com]

(or anywhere else) exactly because it never attains a perfectly symmetric limit-cycle solution ($\Lambda = 0$) at the SB (or anywhere else). The above numerical experiments, detailed in Figures 4A and 4B, hence, follow the rule in Equation (38) and thus fully corroborate and validate the SYM-AM/PM model and specifically the prediction in Equation (35).

In Figure 4A, we see that the THETA-OSC/PAR circuit exhibits a zero-state ($\Upsilon = 0$) directly at the SB for $z_0 = 1$. As mentioned in the introduction, we refer this type of zero-state on the SB as an *ambiguous zero-state* or A-STATE. The A-STATE in Figure 4A is very important for the purpose of verifying the predictions of the SYM-AM/PM model, and this issue was discussed in detail above. However, as we approach the SB, the steady-state oscillator solution, γ, approaches the quiescent DC operating point, with the corresponding oscillation amplitude approaching zero. It hence follows that an A-STATE, such as the one shown in Figure 4A, holds no significant relevance for practical oscillator design.

In contrast, a *proper zero-state*, or P-STATE, refers to a zero-state where the oscillator operates at nonzero power output. The prospect of designing oscillators operating at P-STATES is indeed very interesting as these solution modes represent a local, if not global, minima of the total phase-noise response. Fortunately, with the emergence of the novel SYM-AM/PM model, we, for the first time, have the tools available in order to formulate rules which can be used to guide our design in terms of topology and parameter settings. In the following section, we proceed to apply these newly attained design rules in order to synthesize a novel electrical oscillator circuit which achieves several viable P-STATES.

Figure 5 plots the THETA-OSC oscillator limit-cycle γ and corresponding Floquet vector-bundles $(u_1(\tau), u_2(\tau))$ for various circuit parameter configurations. The figure contains simulations of the THETA-OSC/[PAR/SER] circuits given

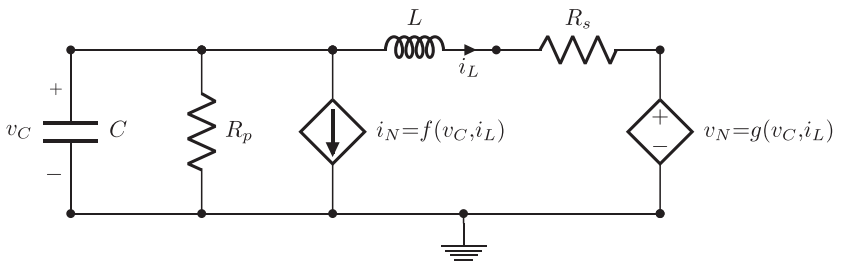

FIGURE 6 The novel SYM-OSC oscillator circuit, synthesized using design guidance attained from the novel SYM-AM/PM model. The circuit contains both a nonlinear transconductance i_N and transimpedance v_N which are defined in Equation (45)

two different parameter configurations, labeled ① and ② (see Figure 5 caption and footnote[‖]). The parameter configuration ① corresponds to the SB for the specific parameter choice $z_0 = 1.0$. For the THETA-OSC/PAR circuit, this operating point corresponds to the A-STATE shown in Figure 4A. The existence of this special state is clearly detected in Figure 5A. Here, the perfectly symmetric limit-cycle and orthogonal Floquet vector-bundle directly corresponds to the singularities in the measures Λ, Υ, defined in Equations (36) and (37), respectively, observed in Figure 4A (blue curves). Figure 5C shows simulations for the same configuration but for the THETA-OSC/SER circuit. The figure clearly illustrates that no such symmetry property holds here and furthermore that the bundle is no longer orthogonal. This again directly corresponds to the lack of an A-STATE (singularity) at the SB for the THETA-OSC/SER circuit in Figure 4B ($z_0 = 1.0$, blue curves). Finally, Figures 5B and 5D shows the equivalent simulations for the THETA-OSC/[PAR/SER] for the parameter configuration ②. Clearly, neither circuit produces a symmetric limit-set in this configuration, and the bundles are also not orthogonal. These results again correlate directly with the curves in Figure 4A–B ($z_0 = 0.7$, turquoise curves). The plots in Figure 5 hence correlate directly with the equivalent curves in Figure 4A–B and hence simply convey a different, perhaps more intuitive, representation of the same results.

5 | SYNTHESIS OF AN OSCILLATOR WITH PROPER ZERO-STATES (P-STATES)

We consider the electrical circuit displayed in Figure 6 which we shall refer to throughout as the SYM-OSC circuit. In order to model this circuit, we proceed to introduce the following two Q-factors:

$$\begin{aligned} Q_p &= \omega_n C R_p \\ Q_s &= \omega_n L / R_s, \end{aligned} \tag{44}$$

where $\omega_n = 1.0/\sqrt{LC}$ is the natural frequency of the circuit resonator. In Figure 6, the controlled sources i_N and v_N have the form

$$\begin{aligned} i_N(v_C, i_L) &= a_1 v_C + a_2 v_C^3 + a_3 i_L^2 v_C \\ v_N(v_C, i_L) &= b_1 i_L + b_2 i_L^3 + b_3 v_C^2 i_L, \end{aligned} \tag{45}$$

where the values and units of the various parameters in the above expressions are listed in Table 1.

Continuous nonlinear functions such as those in Equation (45) can be realized electronically using various different function synthesizer circuit topologies. The perhaps simplest option involves the use of standard op-amp log/anti-log[20,21] and summer circuits which allows for a bare-bone implementation of parametric polynomial functions. Alternatively, operational-transcondutor-amplifier (OTA) circuits can be worked to synthesize any mathematical function characteristic (see, e.g., Sánchez-Sinencio et al[22]). Finally, a dedicated chip such as the AD538[23] can be used to synthesize any polynomial function.

In the following, we normalize the time variable as $\tau = \omega_n t$. The dynamical equations modeling the circuit in Figure 6 can then be written as

[‖]Here, ∼5 mA refers to a value close to, but a little above $I_B = 5$mA which roughly represent the SB for both PAR/SER circuits, for $z_0 = 1.0$, as seen from Equations (42)–(43) and footnote ¶. We hence choose the of value of I_B closest to the SB which still produces a converging limit-cycle solution.

TABLE 1 The values and units of the various parameters in Equation 45

#	Value	Units
a_1	0.6	AV^{-1}
a_2	0.3	AV^{-3}
a_3	0.3	$A^{-1}V^{-1}$
b_1	0.6	VA^{-1}
b_2	0.3	VA^{-3}
b_3	0.3	$A^{-1}V^{-1}$

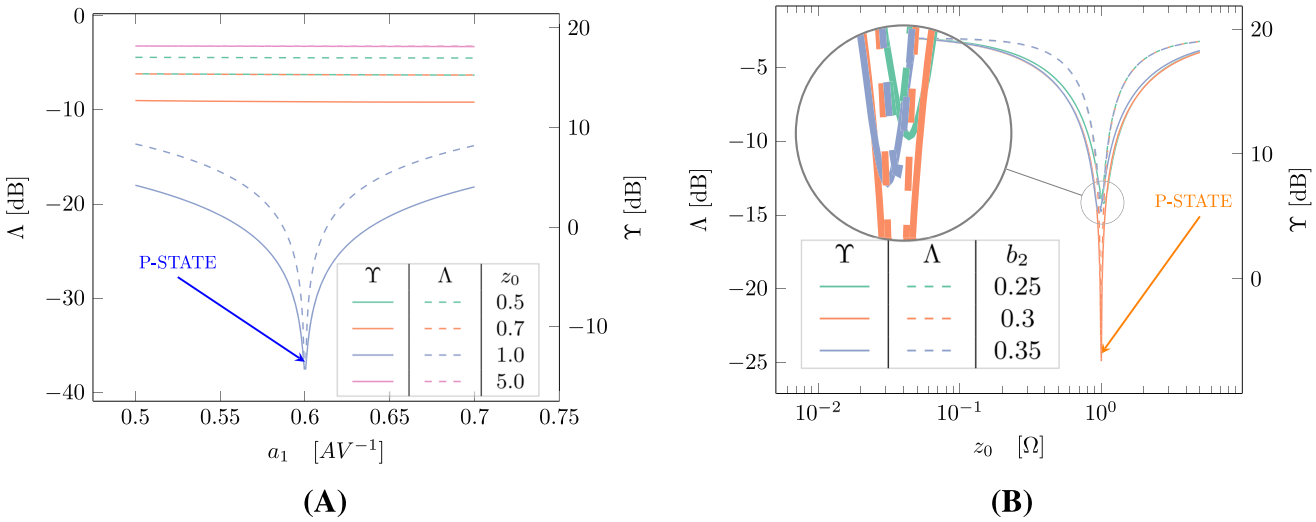

FIGURE 7 Simulations of measures Λ and ϒ, defined in Equations (36) and (37), for the SYM-OSC circuit (see Figure 6) with constant resonator quality factors $Q_p, Q_s = 10$. (A) Sweep of transconductance parameter (linear part) a_1 defined in Equation (46). (B) Sweep of characteristic impedance $z_0 = \sqrt{L/C}$ [Colour figure can be viewed at wileyonlinelibrary.com]

$$\begin{aligned} \dot{x} &= -(z_0/R_p)x - y/z_0 + i_N(xz_0, y/z_0) \\ \dot{y} &= -(R_s/z_0)y + z_0 x + v_N(xz_0, y/z_0), \end{aligned} \tag{46}$$

where $x = v_C/z_0$, $y = i_L z_0$ with $z_0 = \sqrt{L/C}$ being the resonator characteristic impedance, whereas v_C, i_L are the voltage across the capacitor C and current through inductor L, respectively. Note that each set of circuit parameters in Equation (46) corresponds to a unique** component set (C, L, R_p, R_s) in Figure 6.

Figure 7A plots the two measures Λ and ϒ, defined in Equations (36) and (37), for the SYM-OSC in Figure 6 with $Q_p, Q_s = 10.0$. The measures are plotted as a function of the transconductance parameter a_1 for four values of the resonator characteristic impedance z_0. Here, the parameter a_1 describes the linear part of the transconductance i_N defined in Equation (45) with the value of the remaining transconductance and transimpedance parameters being kept fixed to the values displayed in Table 1. Each curve represents a unique set of the SYM-OSC circuit parameters introduced in Figure 6 as explained in footnote **. The figure displays a clear zero-state at the point $a_1 = 6, z_0 = 1$. As discussed in the introduction, since this operating point is located away from the SB, we are dealing with a so-called *proper zero-state* also referred to here as a P-STATE.

Figure 7B again plots the two measures Λ and ϒ for the SYM-OSC in Figure 6 with $Q_p, Q_s = 10.0$. This time as a function of the resonator characteristic impedance $z_0 = \sqrt{L/C}$ and for three values of the transimpedance parameter b_2. Here, the parameter b_2 describes the cubic part of the transimpedance v_N defined in Equation (45) with the value of the

**Throughout, we shall assume that the Q-factors in Equation (44) are fixed, and the corresponding parallel and series loads in Figure 6 are then derived as $R_p = Q_p/(\omega_n C) = Q_p z_0$ and $R_s = \omega_n L/Q_s = z_0/Q_s$. Likewise, the capacitance C and inductance L are easily derived from the circuit parameters as explained in footnote #.

remaining transconductance and transimpedance parameters being kept fixed to the values displayed in Table 1. Each plot point in this figure corresponds to a unique set of SYM-OSC circuit parameters as explained in footnote **. The figure reveals a clear zero-state at the point $z_0 = 1, b_2 = 0.3$, and again, we are dealing with a P-STATE.

The curves in Figure 7A,B all fully corroborate and validate the SYM-AM/PM model discussed in Section 3. Both zero-states in two above figures follow the prediction in Equation (35) as formulated in terms of Υ and Λ in Equation (38). Importantly, we never observe behavior diverging from this rule (e.g., we never observe $\Upsilon \to 0 \wedge \Lambda \not\to 0$). Furthermore, as was noted, both of the zero-states in the above figures are so-called P-STATES which implies an operating point away from the SB. Hence, in both cases, we are able to achieve a zero-state while operating the oscillator at nonzero output-power. This is in stark contrast to the MOSFET oscillator example detailed in the previous section which could only attain an ambiguous zero-state (A-STATE). We are still in the early stages of exploring and discovering all the implications which follow from the novel SYM-AM/PM framework developed in Djurhuus and Krozer.[13] The above results for the SYM-OSC circuit, coupled with an upcoming expansion to higher dimensions currently being prepared for publication, clearly demonstrate the promise of this framework for the purpose of synthesis of practical oscillator designs with the optimized phase-noise response.

The ideas discussed herein open the door on a new class of numerical algorithms aimed at optimizing the phase-noise performance of free-running oscillators. Our work details a novel link between the noise performance of an autonomous oscillator system and symmetry properties of the underlying nonlinear steady-state oscillator solution. This insight allows us to understand which directions in oscillator parameter-space will lead to improved noise performance. Our work shows that these are the directions which lead to an increase in symmetry of the steady-state where full symmetry correspond to a fully optimized state (i.e., a zero-state). Knowing the zeros of the optimizing measure is a necessary component in the formulation of these types of routines. Work is currently ongoing in this area, and we plan to publish our results in the near future.

6 | CONCLUSION

The paper investigates the many interesting practical implications of the newly proposed SYM-AM/PM model framework. A prominent prediction which has emerged from this work is that, for the case of 2-D (planar) oscillators, only circuit topologies generating perfectly symmetric steady-states can have zero AM-PM noise conversion, the so-called *zero-states*. The concept of zero-states is an interesting topic for practical oscillator design as they represent a minimum which is at least local, if not global, for the total oscillator phase-noise response.

The paper includes simulation results for the important example of a MOSFET differential-pair LC oscillator circuit which is a unit found in most modern RF and μ-wave systems. The various simulations all unequivocally verified the correctness of every prediction made by the SYM-AM/PM model. In addition, these simulations showed that zero-states, for this class of transistor circuits, were only possible at the start-up boundaries (SB) where the oscillator solution bifurcates from the DC operating point, so-called A-STATES. These zero-states are only interesting from a verification point-of-view and do not translate into practical oscillator design solutions.

In an effort to remedy this situation, and to illustrate the power of the newly acquired design rules which follow from the SYM-AM/PM framework, we demonstrated the synthesis of a novel reduced-order LC oscillator circuit, known as the SYM-OSC circuit, which attained these zero-states while operating at nonzero output power, so-called P-STATES. This circuit was synthesized entirely by following the instructions, rules, and predictions derived from the novel SYM-AM/PM model framework. The developed SYM-OSC example clearly illustrates how this new theory can be used the synthesize practical oscillator solutions which attain zero-states while operating at realistic output-power levels (P-STATES). The work detailed herein furthermore clearly demonstrate a possible path toward the eventually development of novel numerical algorithms, based on the SYM-AM/PM model, aimed optimizing oscillator phase-noise performance.

ACKNOWLEDGMENT

The authors gratefully acknowledge partial financial support by German Research Foundation (DFG) (Grant KR 1016/16-1). Open access funding enabled and organized by Projekt DEAL.

DATA AVAILABILITY STATEMENT

Research data are not shared.

ORCID

Torsten Djurhuus https://orcid.org/0000-0003-1916-7647

REFERENCES

1. Razavi B. A study of phase noise in CMOS oscillators. *IEEE J Solid-State Circ*. 1996;31(3):331–343.
2. Samori C, Lacaita AL, Villa F, Zappa F. Spectrum folding and phase noise in LC tuned oscillators. *IEEE Trans Circ Syst II Analog Dig Sig Proc*. 1998;45(7):781-790.
3. Laloue A, Nallatamby JC, Prigent M, Camiade M, Obregon J. An efficient method for nonlinear distortion calculation of the AM and PM noise spectra of FMCW radar transmitters. *IEEE Trans Micro Theory Tech*. 2003;51(8):1966-1976.
4. Chang HC, Cao X, Mishra UK, York RA. Phase noise in coupled oscillators: theory and experiment. *IEEE Trans Micro Theory Tech*. 1997;45(5):604-615.
5. Bonnin M, Corinto F, Gilli M. Phase space decomposition for phase noise and synchronization analysis of planar nonlinear oscillators. *IEEE Trans Circ Syst II Exp Briefs*. 2012;59(10):638-642.
6. Bonnin M, Corinto F. Influence of noise on the phase and amplitude of second-order oscillators. *IEEE Trans Circ Syst II Exp Briefs*. 2014;61(3):158-162.
7. Traversa FL, Bonani F. Oscillator noise: a nonlinear perturbative theory including orbital fluctuations and phase-orbital correlation. *IEEE Trans Circ Syst I Reg Papers*. 2011;58(10):2485-2497.
8. Djurhuus T, Krozer V, Vidkjar J, Johansen TK. Trade-off between phase-noise and signal quadrature in unilaterally coupled oscillators. In: IEEE; 2005:4.
9. Djurhuus T, Krozer V, Vidkjær J, Johansen TK. Nonlinear analysis of a cross-coupled quadrature harmonic oscillator. *IEEE Trans Circ Syst I Reg Papers*. 2005;52(11):2276-2285.
10. Demir A, Mehrotra A, Roychowdhury J. Phase noise in oscillators: a unifying theory and numerical methods for characterization. *IEEE Trans Circ Syst I Fund Theory Appl*. 2000;47(5):655-674.
11. Djurhuus T, Krozer V, Vidkjær J, Johansen TK. Oscillator phase noise: a geometrical approach. *IEEE Trans Circ Syst I Reg Papers*. 2009;56(7):1373-1382.
12. Kärtner FX. Analysis of white and f- α noise in oscillators. *Int J Circ Theory Appl*. 1990;18(5):485-519.
13. Djurhuus T, Krozer V. Conditions for an orthogonal floquet decomposition of the oscillator linear response. *SIAM J Appl Dyn Syst (SIADS)*. in review.
14. Swain RS, Gleeson JP, Kennedy MP. Influence of noise intensity on the spectrum of an oscillator. *IEEE Trans Circ Syst II Exp Briefs*. 2005;52(11):789-793.
15. O'Doherty F, Gleeson JP. Phase diffusion coefficient for oscillators perturbed by colored noise. *IEEE Trans Circ Syst II Exp Briefs*. 2007;54(5):435-439.
16. Bonnin M, Corinto F. Phase noise and noise induced frequency shift in stochastic nonlinear oscillators. *IEEE Trans Circ Syst I Reg Papers*. 2013;60(8):2104-2115.
17. Bonnin M. Amplitude and phase dynamics of noisy oscillators. *Int J Circ Theory Appl*. 2017;45(5):636-659.
18. Hajimiri A, Lee TH. Design issues in CMOS differential LC oscillators. *IEEE J Solid-State Circ*. 1999;34(5):717-724.
19. Pepe F, Andreani P. Still more on the f^2 phase noise performance of harmonic oscillators. *IEEE Trans Circ Syst II Exp Briefs*. 2016;63(6):538-542.
20. Wikipedia contributors. Operational amplifier applications—Wikipedia, The Free Encyclopedia. [Online; accessed 23-July-2020]; 2020.
21. Devices A. Inc.ŞMT-077 TutorialU˙Log Amp Basics.Ť; 2012.
22. Sánchez-Sinencio E, Ramirez-Angulo J, Linares-Barranco B, Rodriguez-Vázquez A. Operational transconductance amplifier-based nonlinear function syntheses. *IEEE J Solid State Circ*. 1989;24(6):1576-1586.
23. AD538. Real-time analog computational unit data sheet (Rev E); 2011.

How to cite this article: Djurhuus T, Krozer V. A study of amplitude-to-phase noise conversion in planar oscillators. *Int J Circ Theor Appl*. 2021;49:1–17. https://doi.org/10.1002/cta.2893

APPENDIX A: PROOF OF COROLLARY 2.2.

Using the expression in Equation (23) for the noise vector ξ, we can calculate

$$\begin{aligned}&\left\langle \xi(\tau)\xi^{\dagger}(\tau)\right\rangle = \\ &\left\langle \left([\rho(\tau)+\lambda(\tau)]u_1(\tau)s(\tau)+\sum\nolimits_{k=2}^{n}\nu_{k-1}(\tau)u_k(\tau)s(\tau)\right)\times\right. \\ &\left.\left([\rho(\tau)+\lambda(\tau)]u_1^{\dagger}(\tau)s(\tau)+\sum\nolimits_{k=2}^{n}\nu_{k-1}(\tau)u_k^{\dagger}(\tau)s(\tau)\right)\right\rangle = \\ &(\rho(\tau)+\lambda(\tau))^2u_1(\tau)u_1^{\dagger}(\tau)+\Gamma(\tau)+\Omega(\tau),\end{aligned} \tag{A1}$$

where, as explained in connection with Equation (23), $\{\nu_k(\tau)\}$ are the $n-1$ components of the amplitude noise whereas $\rho(\tau)$ and $\lambda(\tau)$ represent the PM/AM-noise contributions to the phase-mode, respectively. The above expression includes the introduction of two matrix functions

$$\begin{aligned}\Gamma(\tau) &= \sum\nolimits_{j=2}^{n}[\rho(\tau)+\lambda(\tau)]\nu_{j-1}(\tau)\left(u_1(\tau)u_j^{\dagger}(\tau)+u_j(\tau)u_1^{\dagger}(\tau)\right)\\ \Omega(\tau) &= \sum\nolimits_{j=2}^{n}\sum\nolimits_{k=2}^{n}\nu_{j-1}(\tau)\nu_{k-1}(\tau)u_j(\tau)u_k^{\dagger}(\tau),\end{aligned} \tag{A2}$$

and we have used that the noise source $s(\tau)$ is a zero-mean, $<s(\tau)>=0$, and unit-variance, $<s^2(\tau)>=1$, Gaussian white noise source. Since both matrices Γ and Ω in Equation (A2) contains terms containing vectors $u_{j>1}(\tau), u_{j>1}^{\dagger}(\tau)$, it follows directly (see Equation (4) and text in Section 2.2) that

$$v_1^{\dagger}(\tau)\Gamma(\tau)v_1(\tau)=v_1^{\dagger}(\tau)\Omega(\tau)v_1(\tau)=0 \text{ for all } \tau. \tag{A3}$$

From the definition of the phase-diffusion D (16), and the above results in Equations (A1)–(A3), we can calculate

$$D=\frac{1}{2\pi}\int_0^{2\pi}v_1^{\dagger}(s)\langle\zeta(s)\zeta^{\dagger}(s)\rangle v_1(s)ds=\sigma_{\rho\rho}+\sigma_{\lambda\lambda}+2\sigma_{\rho\lambda}, \tag{A4}$$

where

$$\sigma_{xy}=\frac{1}{2\pi}\int_0^{2\pi}x(s)y(s)ds. \tag{A5}$$

Using the decomposition of D introduced in Equation (18) of Section 2.4, we can then write

$$D_{\phi\phi}=\sigma_{\rho\rho}, \tag{A6}$$

$$D_{\phi a}=\sigma_{\lambda\lambda}+2\sigma_{\rho\lambda}, \tag{A7}$$

and we see that $\lambda=0\Leftrightarrow\sigma_{\lambda\lambda}=\sigma_{\rho\lambda}=0\Leftrightarrow D_{\phi a}=0$.